ACS APPLIED MATERIALS & INTERFACES

Research Article

www.acsami.org

Monitoring N3 Dye Adsorption and Desorption on TiO_2 Surfaces: A Combined QCM-D and XPS Study

Hannah K. Wayment-Steele,[†] Lewis E. Johnson,*[,†,∥] Fangyuan Tian,[§] Matthew C. Dixon,[‡] Lauren Benz,[§] and Malkiat S. Johal*[,†]

[†]Department of Chemistry, Pomona College, 645 North College Ave, Claremont, California 91711, United States

[‡]Biolin Scientific, 514 Progress Drive, Suite G, Linthicum Heights, Maryland 21090, United States

[§]Department of Chemistry, University of San Diego, 5998 Acalá Park, San Diego, California 92110, United States

[∥]Department of Chemistry, University of Washington, 109 Bagley Hall, Seattle, Washington 98195, United States

Supporting Information

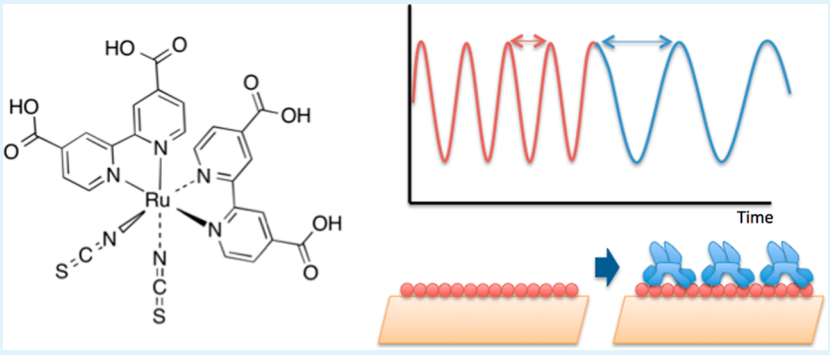

ABSTRACT: Understanding the kinetics of dye adsorption and desorption on semiconductors is crucial for optimizing the performance of dye-sensitized solar cells (DSSCs). Quartz crystal microbalance with dissipation monitoring (QCM-D) measures adsorbed mass in real time, allowing determination of binding kinetics. In this work, we characterize adsorption of the common RuBipy dye N3 to the native oxide layer of a planar, sputter-coated titanium surface, simulating the TiO_2 substrate of a DSSC. We report adsorption equilibrium constants consistent with prior optical measurements of N3 adsorption. Dye binding and surface integrity were also verified by scanning electron microscopy, energy-dispersive X-ray spectroscopy, and X-ray photoelectron spectroscopy (XPS). We further study desorption of the dye from the native oxide layer on the QCM sensors using tetrabutylammonium hydroxide (TBAOH), a commonly used industrial desorbant. We find that using TBAOH as a desorbant does not fully regenerate the surface, though little ruthenium or nitrogen is observed by XPS after desorption, suggesting that carboxyl moieties of N3 remain bound. We demonstrate the native oxide layer of a titanium sensor as a valid and readily available planar TiO_2 morphology to study dye adsorption and desorption and begin to investigate the mechanism of dye desorption in DSSCs, a system that requires further study.

KEYWORDS: *dye-sensitized solar cells, ruthenium dyes, surface characterization, quartz crystal microbalance, Langmuir isotherm*

INTRODUCTION

Dye-sensitized solar cells (DSSCs) have received much attention over the past two decades due to their potential as a less expensive and more environmentally friendly alternative to traditional solar cells.[1] While currently demonstrating lower efficiencies than crystalline silicon cells, in the range of 10%, DSSCs have several potential advantages over current commercial cells, including avoiding the use of high-grade silicon and generation of hazardous waste.[1,2] DSSC efficiencies have increased over the past few years; Grätzel and co-workers recently achieved an efficiency of 12.3%,[3] although further optimization is needed to improve commercial viability.

The primary mechanism by which the DSSC generates current is via a wide-bandgap semiconducting layer, typically TiO_2, at the photoanode, which is sensitized by a layer of adsorbed dye that absorbs strongly at visible wavelengths.[4] Incident light excites the dye; the excited electron is then transferred to the conduction band of the semiconductor and collected by the photoanode. The oxidized dye is reduced to its original state by a redox electrolyte pair such as I^-/I_3^-. The morphology of the dye layer is crucial to optimizing the efficiency of this process. The most desirable dye loading is a monolayer, with complete surface coverage and no aggregation. Aggregation decreases the efficiency of charge carrier transfer

Received: February 12, 2014
Accepted: May 21, 2014
Published: May 21, 2014

by increasing the probability of nonproductive transfer to other dye molecules.[5] Furthermore, direct contact between the semiconductor and the electrolyte solution allows recombination of conduction band electrons via the redox couple, which decreases efficiency by preventing electrons from reaching the photoanode. Maximum surface coverage of the dye is necessary for it to act as a blocking layer to prevent recombination between the semiconductor and electrolyte.[6] Since optimizing surface coverage according to the above conditions would greatly increase device photoconversion efficiency, a more thorough understanding of the dye adsorption process is needed.[7] As the adsorption process depends on many factors, including dye structure/binding orientation, surface chemistry, surface morphology, and solvent conditions, parallel and low-cost methods are greatly beneficial for further optimization of dye/surface pairings.

Knowledge of desorption kinetics is also beneficial for optimizing dye loading. Strong bases[8,9] with high solubility in polar organic solvents, such as tetrabutyl ammonium hydroxide (TBAOH) and tetramethylammonium hydroxide (TMAOH), are used to desorb dye in studies of DSSC performance and function. Bases have been used to partially desorb dye from a monolayer to create a layer of uniform partial coverage, which is useful for studying recombination rates.[10] Bases have also been used in cyclic adsorption and desorption of dye from TiO_2 substrates, which has been shown to increase the efficiency of the device after readsorption,[11] as well as increase the total coverage of the dye.[7] Although strong bases are used as desorbants in these contexts, the mechanism by which they desorb N3 dye is not fully understood at the molecular level.

Surface adsorption and desorption phenomena can be studied in real time using techniques such as quartz crystal microbalance with dissipation monitoring (QCM-D),[12] surface plasmon resonance (SPR),[13] attenuated total reflection infrared spectroscopy (ATR-FTIR),[14] and dual-polarization interferometry.[15] We use the QCM-D technique, which enables time-dependent determination of the thermodynamics and kinetics of an adsorption or desorption process and viscoelastic properties of the resulting film.[12] QCM-D is based on the converse piezoelectric effect, which describes the deformation of a quartz crystal upon the application of an electric potential. When the quartz crystal sensor is subjected to an alternating potential of the appropriate frequency, the sensor will oscillate at its resonant frequency. The frequency of oscillation will decrease when material is adsorbed to the surface. In the limit of a rigid, thin film, the frequency change and adsorbed mass can be described linearly with the Sauerbrey equation:[16]

$$\Delta m = \frac{C\Delta f}{n} \tag{1}$$

where C = 17.7 ng Hz^{-1} cm^{-1} for a 5 MHz crystal and n is the overtone number of the resonant frequency of the crystal.

In the QCM-D technique, in contrast to standard QCM, the crystal is driven by a pulsed potential of the appropriate frequency, and the decay of the oscillation amplitude between pulses is measured as a function of time. The rate of decay of the oscillation due to damping caused by the adsorbed layer is related to the viscoelasticity of the adsorbed mass. The energy loss is described as a dimensionless dissipation value:

$$D = \frac{1}{2\pi}\frac{E_{\text{dissipated}}}{E_{\text{stored}}} \tag{2}$$

where $E_{\text{dissipated}}$ is the energy dissipated by the system and E_{stored} is the energy stored in the system. A rigid film exhibits lower dissipation, whereas a film with higher viscoelasticity results in a higher dissipation. If the dissipation is high, that is, the layer is not sufficiently rigid, the Sauerbrey model is no longer valid. If the rigid film approximation is not valid, more complex Voigt models involving frequency and dissipation from multiple overtones must be used to obtain an accurate mass.[17,18] The magnitude of the dissipation can help validate when and when not to use the Sauerbrey relationship. The N3/TiO_2 system yielded thin, rigid films, which could be readily modeled using the Saurbrey equation (see the Supporting Information).

In the present work, we use QCM-D to characterize the binding of *cis*-bis(isothiocyanato)bis(2,2′-bipyridyl-4,4′-dicarboxylato)-ruthenium II (N3), a frequently studied ruthenium bipyridyl (RuBipy) dye, to a planar TiO_2 surface in an ethanol solution. N3 was selected for its role as a widely studied, prototypical high-performance dye.[19] N3 is highly soluble in ethanol, which is commonly used as a solvent in DSSC fabrication. The amorphous native oxide layer of a titanium-coated quartz crystal sensor was used as the substrate. Others have used this native oxide layer as an effective surface to characterize protein adsorption to TiO_2.[20] Furthermore, dye adsorption to atomic layer deposition (ALD)-prepared TiO_2 surfaces has previously been demonstrated using QCM-D.[21] However, ALD-prepared surfaces require a more expensive laboratory setup including vacuum equipment. Using a premanufactured, sputter-deposited titanium QCM-D sensor saves both time and money, allowing for rapid characterization of dye adsorption. We have previously demonstrated proof-of-concept results for adsorption of N3 to the native oxide layer of titanium QCM sensors;[22] this work represents the first systematic characterization of N3 adsorption and desorption on these substrates. We modeled our data using an independent-site binding model, fit it to a Langmuir isotherm, and calculated the binding constant and maximal adsorption per unit area. Our binding constants are in agreement with literature values obtained using other techniques, underscoring the applicability of this technique to studying dye adsorption for DSSC applications. We also studied desorption within the same concentration range, using TBAOH, and demonstrated that exposing a dye-coated TiO_2 substrate to TBAOH does not entirely remove the bound dye but instead leaves residue on the surface. We also demonstrated desorption with acetic acid (AcOH) to show that desorption is not specific to strong bases but is related to a change in the protonation state of the system.

MATERIALS AND METHODS

Materials. *cis*-Bis(isothiocyanato)bis(2,2′-bipyridyl-4,4′-dicarboxylato)-ruthenium(II) (N3) (Solaronix, CAS141460-19-7), 100% ethanol (Sigma–Aldrich, CAS no. 64-17-5), tetrabutylammonium hydroxide (TBAOH) (Fisher Scientific, CAS no. NC0107153), glacial acetic acid (Spectrum, CAS no. 64-19-7), and 0.1 M NaOH (Sigma–Aldrich, CAS no. 1310-73-2) were used as received.

QCM-D. Real-time frequency and dissipation data were collected using a Q-Sense E4 QCM-D instrument (Q-Sense, Gothenburg, Sweden). The instrument is capable of running four simultaneous samples in independent flow cells. The QCM-D sensors, mounted in a liquid flow cell (40 μL), consist of AT-cut piezoelectric quartz crystal disks with a resonant frequency of 4.95 MHz, sputter-coated with a 120 nm layer of titanium metal, with a surface roughness of 1.7 ± 0.2 nm as measured by atomic force microscopy (see the Supporting Information). The titanium was oxidized in air to form a native oxide layer consisting predominantly of TiO_2, with a minority of the

titanium (14%) in the formal +3 oxidization state, as determined by X-ray photoelectron spectroscopy (XPS) (see the Supporting Information). Crystals were treated with a 2 vol % Hellmanex III surfactant solution (Hellma GmbH & Co.) for 30 min, rinsed with reverse osmosis water (Milli-Q, ρ > 18.2 MΩ cm), dried with N_2, sonicated for 10 min in absolute ethanol, rinsed with reverse osmosis water, dried with N_2, and cleaned in a UV/ozone chamber for 10 min before being placed in the QCM-D flow cells. The surface of the TiO_2 crystal was exposed to dye solutions of varying concentrations. A stable baseline was obtained first in reverse osmosis water, followed by absolute ethanol. Dye solutions were then flowed through the chamber according to the experimental design. Each exposure to dye solution was followed by rinsing with absolute ethanol until no change in frequency was observed. Data were acquired using QSoft (Q-Sense), processed using QTools (Q-Sense), and analyzed using Matlab (Mathworks, Inc). The solution concentration of N3 in ethanol was verified with UV−visible (UV−vis) spectroscopy (Varian Cary 300), using λ_{max} = 538 nm and $\varepsilon = 1.47 \times 10^4$ M^{-1} cm^{-1}.[23] Sensors were used for multiple runs, with dye removed by exposure to 2 vol % Hellmanex III solution for 24 h before cleaning as previously described above. The sensors showed no deterioration or increased noise during successive trials.

Ellipsometry. The thickness of the native oxide layer was measured using ellipsometry (L2W16S544 Stokes Ellipsometer, Gaertner Scientific, Chicago, IL, USA) at 632.8 nm assuming a substrate refractive index of $\tilde{n} = 3.00 + 3.62i$ and simultaneously fitting the film index and thickness. The native oxide layer above the titanium metal was measured to be 5.1 ± 0.2 nm by ellipsometry (n = 4).

EDX. Energy-dispersive X-ray spectroscopy (EDX, Thermo Scientific) spectra were collected using scanning electron microscopy (SEM, Hitachi S-3400N) with a secondary electron detector at an accelerating energy of 10 kV. Electron micrographs of the sensor surface were collected using the same instrument and voltage, with current and sample distance tuned for optimum image quality. Samples used for SEM/EDX were prepared on substrates identical to those used for QCM-D, following the same cleaning procedure, but with adsorption and desorption conducted ex situ by immersion in solutions of the appropriate concentration for 5 min.

XPS. XPS spectra (PHI 04-548) were collected with a Mg Kα anode ($h\nu$ = 1253.6 eV). All spectra were collected with a 100 eV pass energy with scan speeds of 0.1−0.5 eV/step. Spectra were calibrated based on the Ti 2p $^3/_2$ peak at 458.4 eV corresponding to Ti^{4+}. Peaks were fit using combined Gaussian−Lorentzian functions using a Shirley background. Samples used for XPS were prepared on substrates identical to those used for QCM-D, following the same cleaning procedure, but with adsorption and desorption conducted ex situ by immersion in solutions of the appropriate concentration for 5 min.

RESULTS AND DISCUSSION

N3 Adsorption. To investigate the kinetics of N3 adsorption to TiO_2, we monitored adsorbed mass as a function of the concentration of dye solution passed through the flow cells. Dye was adsorbed to the surface, resulting in a decrease in frequency until equilibrium was reached. The crystals were then rinsed with absolute ethanol to remove loosely bound/physisorbed dye from the surface; the net frequency drop represents the addition of strongly bound dye (i.e., dye not rapidly removed by an ethanol rinse). Dissipation remained close to zero during the portions of the rinse stage after weakly bound dye was removed. This suggests that dye is strongly coupled to the surface and the adsorbed dye can be modeled as a rigid film, allowing use of the Sauerbrey equation to calculate adsorbed mass.

When sensors were exposed to successively increasing concentrations of dye, the mass of strongly bound dye adsorbed increases until saturation of the surface is reached. Prior ATR-FTIR studies[4] by Nazeeruddin et al. have indicated that N3 chemisorbs to TiO_2 via complexation of Ti^{4+} sites by the carboxylate groups on the ligands. Similar behavior has been observed for other carboxylates.[14,24] While the carboxylate groups bind strongly, with a negligible desorption rate in the absence of acids, bases, or competing ligands, the process is reversible.[24] We modeled the adsorption process with the Langmuir isotherm, which has previously been used to quantify the binding of dye to TiO_2,[25,26] along with other strong binding events such as self-assembled alkanethiol monolayers on gold substrates.[13,27] The Langmuir adsorption equation assumes that binding sites are identical and independent, that the binding is a reversible process, and that there are a finite number of binding sites resulting in monolayer coverage:

$$\Gamma = \Gamma_{max}\frac{Kc}{1 + Kc} \quad (3)$$

In eq 3, the surface concentration Γ is fit as a function of maximum coverage (Γ_{max}), an equilibrium constant (K), and the bulk concentration (c) of the adsorbent.

Figure 1a depicts the mass calculated using the Sauerbrey equation as a function of time from four simultaneous QCM runs upon exposure to successively increasing dye concentrations, with EtOH rinses between to remove weakly bound dye. In Figure 1b, a Langmuir curve was fit to the strongly bound mass data using the nonlinear fit program of Matlab. For calculations, the seventh QCM-D overtone was used due to its favorable signal/noise ratio. Table 1 gives the calculated Γ_{max} and K values for the four flow cells, as well as the root-mean-square error (RMSE) of the fit to the data. The RMSE values are reasonably small that we consider the Langmuir a good approximation of the data.

The equilibrium constants calculated using nonlinear fits are in agreement with equilibrium constants for N3 in ethanol binding to nanocrystalline P25 TiO_2, measured with absorbance (2.8×10^4 M^{-1})[25] and on the same order of magnitude as reported equilibrium constants for the adsorption of N3 to slabs of atomically flat anatase and rutile TiO_2 in ethanol, which were measured using IPCE data ($K_{eq} = 8.0 \times 10^4$ M^{-1}).[26] Our measurements were conducted on a thin native oxide layer that did not exhibit a clear crystal structure, consistent with prior literature.[28−30] Therefore, we expect variation in our measured K_{eq} value compared to those conducted on single-crystal anatase or rutile, but it is promising that these values are on the same order of magnitude of K_{eq} values for other flat TiO_2 substrates. The similarity suggests that the native oxide layer of a Ti sensor in the QCM-D module can be used to simulate dye adsorption to anatase morphologies of TiO_2 used in DSSCs.

Surface composition after exposure to 0.4 mM N3 solution was characterized using XPS. Figure 2 shows the C 1s and Ru 3d regions that reveal the presence of a number of components from the dye. The Ru 3d $^5/_2$ peak at 281.7 eV is a clear indicator that the dye is adsorbed on the surface. The binding energy of this component is consistent with that reported for the related $Ru(bpy)_3$ dye.[31] We also fitted a C 1s peak at 285.4 eV for the pyridine groups of the dye,[31] with an area corresponding to that expected based on stoichiometry and discovered that the presence of additional adventitious carbon at approximately the same energy was required for a good fit. The presence of adventitious carbon is typical of all surfaces exposed to air and was also observed on an untreated sample, along with a weak carbonate peak, which is a common

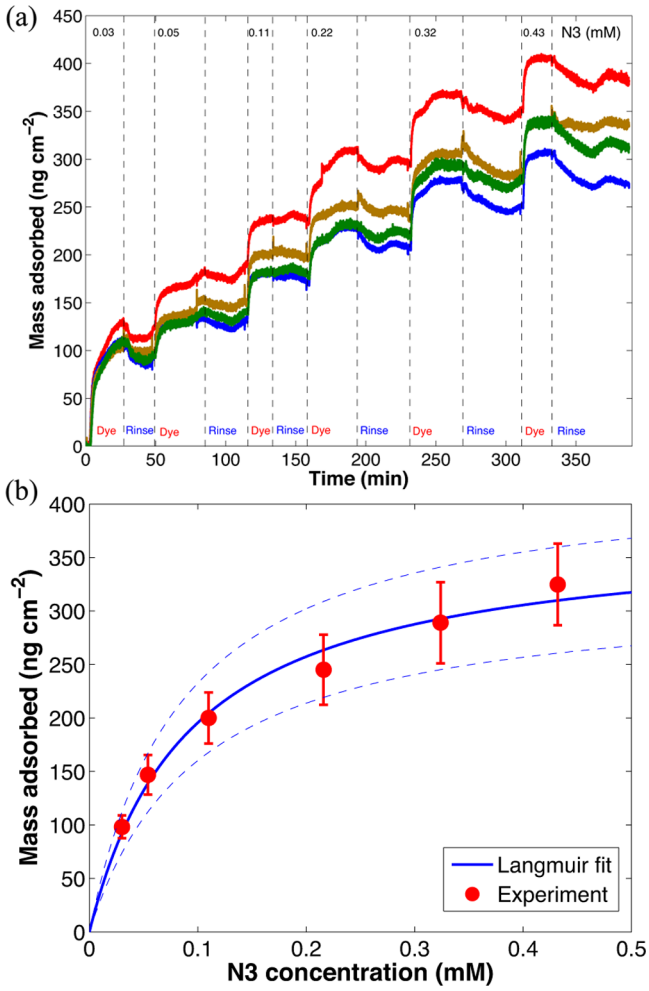

Figure 1. (a) Mass calculated via Sauerbrey equation from frequency data. Average strongly bound mass as a function of dye concentration, as determined from four simultaneous flow cells. Each of the colored lines represents results from an individual flow cell. (b) Average strongly bound mass in four simultaneous flow cells as a function of dye concentration of solution. The solid line indicates a nonlinear least-square fit to the Langmuir model (eq 3). The dashed lines indicate the standard error of the Langmuir fit.

Table 1. Calculated Γ_{max} and K Values Fitting Successive Concentration Adsorption Data to the Langmuir Equation with the Nonlinear Fitting Routines of Matlab

flow cell no.	Γ_{max} (ng cm^{-2})	K (mM^{-1})	RMSE
1	445.1	11.11	6.311
2	314.1	11.99	3.469
3	386.0	10.18	4.978
4	358.8	10.08	4.315
chamber av	376.0	10.84	4.768
std error	54.7	0.89	1.200

contaminant on oxide surfaces.[32] As the surface had been cleaned by UV/O_3 treatment, which has been previously documented[33] to dramatically reduce the presence of adventitious carbon on metal oxide surfaces, it is likely that exposure occurred during transfers before or after dye deposition. The C 1s signal was far weaker for the control sample (Figure 2a) than for the samples exposed to dye (Figure 2b–d). Integration of the C 1s peak and comparison of the O 1s and Ti 2p peaks (spectra are included as Supporting Information) indicated a surface coverage of 17% carbon, with the vast majority of the surface available for dye adsorption. In the samples that had been exposed to dye, the carbon component at 288.0 eV corresponds to the carboxylic groups from the dye and the surface, and a small peak was fit corresponding to carbon in cyano groups at 287.5 eV with proper stoichiometry.

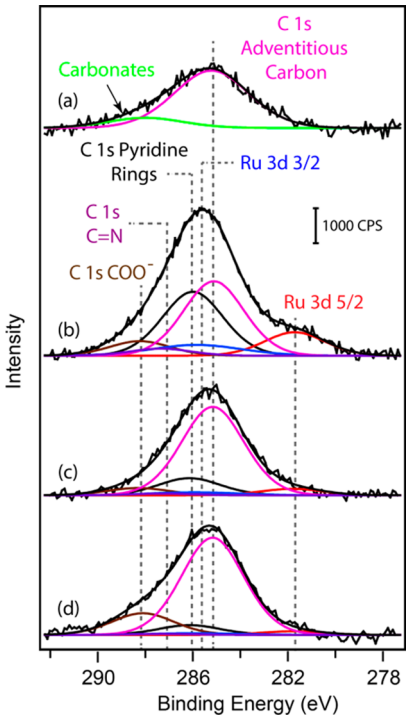

Figure 2. High-resolution C 1s/Ru 3d XPS spectrum of (a) an untreated TiO_2 QCM-D sensor, (b) an N3-treated TiO_2 sensor; (c) an N3-treated sensor following treatment with a TBAOH solution, and (d) an N3-treated sensor following treatment with an AcOH solution. Experimental data was fitted following subtraction of a Shirley background.

N3-modified TiO_2 surfaces were also examined by SEM and EDX (the micrographs and spectra are provided in the Supporting Information) to check for uniformity, and our results indicate that the N3-treated TiO_2 surface is optically smooth; no visible change in roughness was observed using SEM, and no significant defects or aggregation of dye molecules were observed. Ex situ sample preparation mimics the QCM-D flow condition; however, the amount of adsorbed N3 dye was below EDX detection limits. Thus, a second TiO_2 crystal was treated in an N3 solution overnight and then rinsed with absolute ethanol before conducting EDX measurements. Ruthenium, nitrogen, carbon, and titanium signals were observed in EDX in this case, as shown in the Supporting Information.

QCM Studies of N3 Desorption. For desorption studies, the flow cells were baselined in EtOH for 30 min. Each exposure to the solution was continued until the frequency shift stabilized. The approximate durations until frequency equilibrium are given with each step. The flow cells were exposed to dye (20 min), rinsed in EtOH (15 min), exposed to the desorbant (30 min), and again rinsed in EtOH (15 min). The frequency shift for each step was recorded as the strongly bound mass after rinsing in EtOH. Typical Δf and ΔD data for three overtones during this procedure are shown in Figure 3.

dx.doi.org/10.1021/am500920w | ACS Appl. Mater. Interfaces 2014, 6, 9093−9099

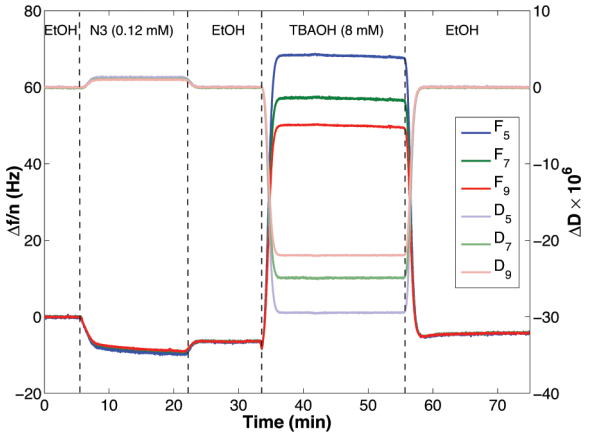

Figure 3. Representative Δf and ΔD data at the fifth, seventh, and ninth overtones for desorption studies. Sensor is exposed to N3 dye, rinsed in EtOH, exposed to TBAOH in EtOH, and rinsed in EtOH. Note that, during dye and EtOH exposure, the overtones are close in Δf and ΔD, indicating N3 binds in a rigid layer. Frequency divergence occurs upon addition of TBAOH. Once the sensors are again rinsed in EtOH, the data for the overtones converge, again indicating a rigidly bound residue.

During the duration of the dye exposure and the first EtOH rinse, the overtones are consistent, which means that the adsorbed mass can be modeled as a rigid mass. When exposed to a solution of TBAOH in EtOH/MeOH, the Δf and ΔD measurements for each overtone diverge. When rinsed in EtOH, they converge to the same value again. This reversible frequency shift and divergence upon the addition of TBAOH is likely due to the density and viscosity differences between the TBAOH solution and EtOH. The shift was observed even in the absence of adsorbed dye and retained full reversibility; the substrate was not affected by the addition of TBAOH solution.

The fraction of bound dye removed increases with the concentration of TBAOH used for desorption. The sensors were exposed to the same concentration of dye in all experiments, but due to the 1−2 Hz variation in the frequency shift upon dye exposure, the mass removed upon desorption was plotted as a percentage of the original mass of dye bound. Figure 4 shows the percent change in mass upon desorption as a function of TBAOH concentration. The fraction of dye desorbed as a function of desorbant concentration can be fit to a logistic curve. The adsorbed mass did not return to baseline even at high TBAOH concentrations, indicating that some material remains on the surface, whether dye bound through a different mechanism, dye−base complex, or dye fragments (e.g. RuO_2), free ligand, or adventitious carbon.

We hypothesize that TBAOH removes N3 dye from the surface through an electrostatic mechanism by increasing the number of deprotonated carboxylate groups, leading to repulsion from the oxide surface, which is negatively charged under basic conditions.[34−36] This was tested with UV−vis spectroscopy. Upon addition of 0.01 M TBAOH to the dye solution, the absorption peaks shifted to shorter wavelengths with no change in magnitude. This is consistent with existing literature on the protonation states of N3 dye[37] (Table 2). Spectra are shown in the Supporting Information.

We also used XPS to monitor the surface following treatment with TBAOH. The ruthenium signal decreased dramatically as shown in Figure 2c, while the most intense signal remaining was from adventitious carbon, which increased by 21%

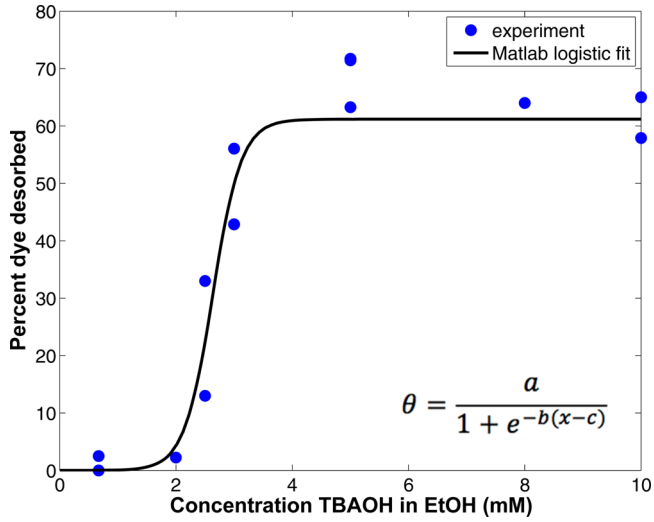

Figure 4. Percent of the mass of bound dye desorbed as a function of desorbant (TBAOH) concentration. Matlab logistic fit is given by the inset equation, where θ is the percent desorbed, x is the TBAOH concentration, and a, b, and c are the fit parameters. Values obtained for the parameters are a = 61.1733, b = 4.074, and c = 2.6343, with RMSE = 6.519.

Table 2. UV−Vis Data for Initial Dye and Deprotonated Dye with Comparison to Literature Values

protonation state	wavelength peaks (nm)
N3 before base	314, 394, 533
lit values $N3H_3^-$ [37]	315, 395, 530
N3 with 0.01 M TBAOH	309, 377, 516
$N3H_3^-$ [37]	310, 380, 515

compared to the nondesorbed sample. This carbon, likely due to dye degradation or electrostatic adsorption of TBA cations, may explain the residual mass on the surface as shown by the QCM results. The reduction of the ruthenium signal corresponds to removal of 75% of the dye.

AcOH Desorption. Desorption of dye is not unique to base but can also be induced using a weak acid. Figure 5 shows the percent of dye desorbed as a function of AcOH dissolved in

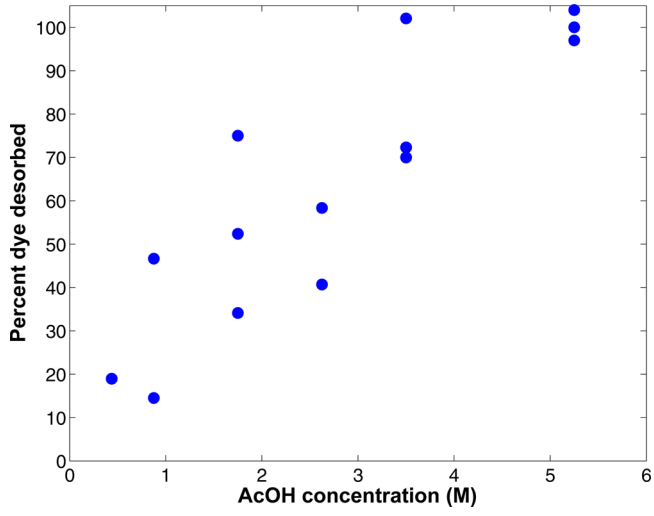

Figure 5. Percent of the mass of bound dye desorbed as a function of desorbant (AcOH) concentration.

dx.doi.org/10.1021/am500920w | ACS Appl. Mater. Interfaces 2014, 6, 9093−9099

EtOH. Much larger concentrations of AcOH were required to observe desorption than for TBAOH, and data were far noisier, not producing a significant fit to a logistic model. Qualitatively, it can be seen that increasing the AcOH concentration removes a higher percent of bound dye.

Upon adding AcOH to N3 solution, the UV−vis absorption peaks showed no change, suggesting that the dye is already in a protonated state prior to desorption. This could be why desorption with TBAOH leaves more residue on the surface. Protonation of the surface leads to a positive surface charge,[24,34] and the protonated surface and positively charged dye may interact less strongly, leading to displacement of the dye upon cleavage of bonds between the carboxylate and Ti^{4+}.

XPS measurements on an AcOH-treated surface are shown in Figure 2d. Similar to the treatment with TBAOH, the Ru nearly disappears, while adventitious C makes up the largest component of the signal. The decrease in the Ru signal corresponds to removal of 84% of the dye. Interestingly, the carboxylate component increases relative to the other two spectra, suggesting possible carboxylate group formation following acid treatment. The total signal from adventitious and carboxylate/carbonate carbon increased by 46% compared to the nondesorbed sample, likely indicating adsorption of the acetic acid to the surface.[24]

N3 Desorption with NaOH. Sodium hydroxide is commonly used to desorb dye. NaOH is known to etch TiO_2, and when TiO_2 sensors were stored in 0.1 M NaOH solution for a period of 3 months, visible etching of the TiO_2 was observed. However, when using 0.01 M NaOH solution in experiments that lasted no longer than 4 h, complete removal of dye was observed without visible damage to the sensor. The QCM frequency shift was also stable after exposure, further suggesting the sensor had not been damaged (see the Supporting Information). Ellipsometry showed no significant change in TiO_2 thickness (initial thickness: 4.94 ± 0.32 nm; final thickness: 4.93 ± 0.65 nm). These results suggest that it is possible to study desorption using dilute mineral bases using QCM-D.

CONCLUSION

We have demonstrated the use of QCM-D to measure the binding of N3 dye to sputter-coated TiO_2, and we report equilibrium constants that are in agreement with spectroscopic methods. We have also validated the use of the native oxide layer of titanium metal to characterize dye adsorption to TiO_2. The native oxide layer of a titanium sensor is much more readily available than other TiO_2 substrates, such as ALD-deposited nanocrystalline titania, and therefore provides a facile setup to further study other aspects of dye adsorption and desorption. We have investigated desorption of N3 from a planar TiO_2 surface in QCM-D using TBAOH, a strong base commonly used for dye desorption in DSSC studies. We have shown that mass remains on the surface after overlaying TBAOH. Although the exact nature of this remaining mass needs further investigation, its presence may pose problematic for the use of TBAOH as a desorbant, since it does not completely remove the N3 dye. We have also shown that desorption is not unique to strong bases but that weak acids can also be used to desorb N3 at high concentrations. Although uncertainties in the mechanism of TBAOH desorption remain, QCM-D was shown to be a viable tool in better understanding adsorption and desorption phenomena for DSSC-relevant dyes and may be useful for future study of novel compounds and device architectures.

ASSOCIATED CONTENT

Supporting Information

Electron micrographs and EDX spectra of the QCM sensor surfaces, XPS survey spectra, UV−vis spectra for N3 exposed to each of the desorbants, additional Ti and O XPS data, and additional QCM data. This material is available free of charge via the Internet at http://pubs.acs.org.

AUTHOR INFORMATION

Corresponding Authors

*(L.E.J.) E-mail: lewisj@uw.edu.

*(M.S.J.) E-mail: malkiat.johal@pomona.edu.

Notes

The authors declare the following competing financial interest(s): MCD is employed by Biolin Scientific, which manufactures QCM-D instrumentation. All other authors declare no competing financial interest..

ACKNOWLEDGMENTS

The authors thank the Pomona College Department of Chemistry, the Department of Chemistry and Biochemistry at the University of San Diego, and the Henry Luce Foundation's Clare Boothe Luce Program for financial support, and Biolin Scientific for material and technical support. L.B. and F.T. thank Aileen Park (USD) for technical assistance, and L.E.J. thanks William Crane (Pomona) for technical assistance and Jason Sellers (UW) for useful discussion.

REFERENCES

(1) O'Regan, B.; Grätzel, M.; Low-Cost, A. High-Efficiency Solar Cell Based on Dye-Sensitized Colloidal TiO_2 Films. *Nature* **1991**, *353*, 737−740.

(2) Greijer, H.; Karlson, L.; Lindquist, S. E.; Hagfeldt, A. Environmental Aspects of Electricity Generation from a Nanocrystalline Dye Sensitized Solar Cell System. *Renewable Energy* **2001**, *23*, 27−39.

(3) Yella, A.; Lee, H. W.; Tsao, H. N.; Yi, C. Y.; Chandiran, A. K.; Nazeeruddin, M. K.; Diau, E. W. G.; Yeh, C. Y.; Zakeeruddin, S. M.; Gratzel, M. Porphyrin-Sensitized Solar Cells with Cobalt (II/III)-Based Redox Electrolyte Exceed 12 Percent Efficiency. *Science* **2011**, *334*, 629−634.

(4) Nazeeruddin, M. K.; Humphry-Baker, R.; Liska, P.; Grätzel, M. Investigation of Sensitizer Adsorption and the Influence of Protons on Current and Voltage of a Dye-Sensitized Nanocrystalline TiO_2 Solar Cell. *J. Phys. Chem. B* **2003**, *107*, 8981−8987.

(5) Grätzel, M. The Advent of Mesoscopic Injection Solar Cells. *Prog. Photovoltaics* **2006**, *14*, 429−442.

(6) Ardo, S.; Meyer, G. J. Photodriven Heterogeneous Charge Transfer with Transition-Metal Compounds Anchored to TiO_2 Semiconductor Surfaces. *Chem. Soc. Rev.* **2009**, *38*, 115−164.

(7) Bazzan, G.; Deneault, J. R.; Kang, T.-S.; Taylor, B. E.; Durstock, M. F. Nanoparticle/Dye Interface Optimization in Dye-Sensitized Solar Cells. *Adv. Funct. Mater.* **2011**, *21*, 3268−3274.

(8) Harlow, G. A.; Noble, C. M.; Wyld, G. E. A. Potentiometric Titration of Very Weak Acids: Tetrabutylammonium Hydroxide as Titrant in Nonaqueous Media. *Anal. Chem.* **1956**, *28*, 787−791.

(9) Deal, V. Z.; Wyld, G. A. Potentiometric Titration of Very Weak Acids: Titration with Hydroxides in Nonaqueous Media Using Glass-Calomel Electrode System. *Anal. Chem.* **1955**, *27*, 47−55.

(10) O'Regan, B.; Li, X. E.; Ghaddar, T. Dye Adsorption, Desorption, and Distribution in Mesoporous TiO_2 Films, and Its Effects on

Recombination Losses in Dye Sensitized Solar Cells. *Energy Environ. Sci.* **2012**, *5*, 7203−7215.
(11) Chiang, Y. F.; Chen, R. T.; Shen, P. S.; Chen, P.; Guo, T. F. Extension Lifetime for Dye-Sensitized Solar Cells through Multiple dye Adsorption/Desorption Process. *J. Power Sources* **2013**, *225*, 257−262.
(12) Rodahl, M.; Hook, F.; Kasemo, B. QCM Operation in Liquids: An Explanation of Measured Variations in Frequency and Q Factor with Liquid Conductivity. *Anal. Chem.* **1996**, *68*, 2219−2227.
(13) Peterlinz, K. A.; Georgiadis, R. In Situ Kinetics of Self-Assembly by Surface Plasmon Resonance Spectroscopy. *Langmuir* **1996**, *12*, 4731−4740.
(14) Roncaroli, F.; Blesa, M. A. Kinetics of Adsorption of Carboxylic Acids onto Titanium Dioxide. *Phys. Chem. Chem. Phys.* **2010**, *12*, 9938−9944.
(15) Swann, M. J.; Peel, L. L.; Carrington, S.; Freeman, N. J. Dual-Polarization Interferometry: An Analytical Technique to Measure Changes in Protein Structure in Real Time, to Determine the Stoichiometry of Binding Events, and to Differentiate Between Specific and Nonspecific Interactions. *Anal. Biochem.* **2004**, *329*, 190−198.
(16) Sauerbrey, G. Verwendung von Schwingquarzen zur Wägung dünner Schichten und zur Mikrowägung. *Z. Physik* **1959**, *155*, 206−222.
(17) Vogt, B. D.; Lin, E. K.; Wu, W.; White, C. C. Effects of Film Thickness on the Validity of the Sauerbrey Equation for Hydrated Polyelectrolyte Films. *J. Phys. Chem. B* **2004**, *108*, 12685−12690.
(18) Voinova, M. V.; Jonson, M.; Kasemo, B. 'Missing Mass' Effect in Biosensor's QCM Applications. *Biosens. Bioelectron.* **2002**, *17*, 835−841.
(19) Nazeeruddin, M. K.; Kay, A.; Rodicio, I.; Humphrybaker, R.; Muller, E.; Liska, P.; Vlachopoulos, N.; Gratzel, M. Conversion of Light to Electricity by *cis*-X_2Bis(2,2′-bipyridyl-4,4′-dicarboxylate)-ruthenium(II) Charge-Transfer Sensitizers (X = Cl^-, Br^-, I^-, CN^-, and SCN^-) on Nanocrystalline TiO_2 Electrodes. *J. Am. Chem. Soc.* **1993**, *115*, 6382−6390.
(20) Van De Keere, I.; Svedhem, S.; Hogberg, H.; Vereecken, J.; Kasemo, B.; Hubin, A. In Situ Control of the Oxide Layer on Thermally Evaporated Titanium and Lysozyme Adsorption by Means of Electrochemical Quartz Crystal Microbalance with Dissipation. *ACS Appl. Mater. Interfaces* **2009**, *1*, 301−310.
(21) Harms, H. A.; Tétreault, N.; Gusak, V.; Kasemo, B.; Grätzel, M. In Situ Investigation of Dye Adsorption on TiO_2 Films Using a Quartz Crystal Microbalance with a Dissipation Technique. *Phys. Chem. Chem. Phys.* **2012**, *14*, 9037−9040.
(22) Wayment-Steele, H. K.; Johnson, L. E.; Dixon, M. C.; Johal, M. S. Characterization of N3 Dye Adsorption on TiO_2 Using Quartz-Crystal Microbalance with Dissipation Monitoring. *Proc. SPIE* **2013**, 8823.
(23) Fantai, K.; Songyuan, D.; Kongjia, W. Purification of Bipyridyl Ruthenium Dye and Its Application in Dye-Sensitized Solar Cells. *Plasma Sci. Technol.* **2006**, *8*, 531−534.
(24) Blesa, M. A.; Weisz, A. D.; Morando, P. J.; Salfity, J. A.; Magaz, G. E.; Regazzoni, A. E. The Interaction of Metal Oxide Surfaces with Complexing Agents Dissolved in Water. *Coord. Chem. Rev.* **2000**, *196*, 31−63.
(25) Fillinger, A.; Parkinson, B. A. The Adsorption Behavior of a Ruthenium-Based Sensitizing Dye to Nanocrystalline TiO_2 Coverage Effects on the External and Internal Sensitization Quantum Yields. *J. Electrochem. Soc.* **1999**, *146*, 4559−4564.
(26) Lu, Y.; Choi, D.-j.; Nelson, J.; Yang, O. B.; Parkinson, B. A. Adsorption, Desorption, and Sensitization of Low-Index Anatase and Rutile Surfaces by the Ruthenium Complex Dye N3. *J. Electrochem. Soc.* **2006**, *153*, E131.
(27) Schessler, H. M.; Karpovich, D. S.; Blanchard, G. J. Quantitating the Balance between Enthalpic and Entropic Forces in Alkanethiol/Gold Monolayer Self Assembly. *J. Am. Chem. Soc.* **1996**, *118*, 9645−9651.
(28) Lu, G.; Bernasek, S. L.; Schwartz, J. Oxidization of a Polycrystalline Titanium Surface by Oxygen and Water. *Surf. Sci.* **2000**, *458*, 80−90.
(29) Leprince-Wang, Y.; Yu-Zhang, K. Study of the Growth Morphology of TiO_2 Thin Films by AFM and TEM. *Surf. Coat. Technol.* **2001**, *140*, 155−160.
(30) Fadl-allah, S. A.; Mohsen, Q. Characterization of Native and Anodic Oxide Films Formed on Commercial Pure Titanium Using Electrochemical Properties and Morphology Techniques. *Appl. Surf. Sci.* **2010**, *256*, 5849−5855.
(31) Susac, D.; Kono, M.; Wong, K. C.; Mitchell, K. A. R. XPS Study of Interfaces in a Two-Layer Light-Emitting Diode Made from PPV and Nafion with Ionically Exchanged $Ru(bpy)_3^{2+}$. *Appl. Surf. Sci.* **2001**, *174*, 43−50.
(32) Barr, T. L. Nature of the Use of Adventitious Carbon as a Binding Energy Standard. *J. Vac. Sci. Technol., A* **1995**, *13*, 1239−1246.
(33) Engelhard, M.; Herman, J.; Wallace, R.; Baer, D. As-Received, Ozone Cleaned and Ar^+ Sputtered Surfaces of Hafnium Oxide Grown by Atomic Layer Deposition and Studied by XPS. *Surf. Sci. Spectra* **2011**, *18*, 46−57.
(34) Jansuz, W.; Sworska, A.; Szczypa, J. The Structure of the Electrical Double Layer at the Titanium Dioxide/Ethanol Solutions Interface. *Colloids Surf., A* **1999**, *152*, 223−233.
(35) Yates, D. A.; Healy, T. W. Titanium Dioxide-Electrolyte Interface. *J. Chem. Soc., Faraday Trans. 1* **1980**, *76*, 9−18.
(36) Holmberg, J. P.; Ahlberg, E.; Bergenholtz, J.; Hassellov, M.; Abbas, Z. Surface Charge and Interfacial Potential of Titanium Dioxide Nanoparticles: Experimental and Theoretical Investigations. *J. Colloid. Interface Sci.* **2013**, *407*, 168−176.
(37) Pizzoli, G.; Lobello, M. G.; Carlotti, B.; Elisei, F.; Nazeeruddin, M. K.; Vitillaro, G.; De Angelis, F. Acid-Base Properties of the N3 Ruthenium(II) Solar Cell Sensitizer: A Combined Experimental and Computational Analysis. *Dalton Trans.* **2012**, *41*, 11841−11848.